Numerical investigation and design of aluminium alloy channel section columns at elevated temperatures

DOI:
10.1016/j.tws.2020.107225

Document Version
Accepted author manuscript

Ji-Hua Zhu, Zi-qi Li and Mei-Ni Su, (2020) "Numerical investigation and design of aluminium alloy channel section columns at elevated temperatures", Thin-walled Structures, 107225.

Numerical investigation and design of aluminium alloy channel section columns at elevated temperatures

Ji-Hua Zhu[1], Zi-qi Li[1] and Mei-Ni Su[2]*

[1] Department of Civil Engineering, Shenzhen University, Shenzhen, China
[2] *School of Mechanical, Aerospace and Civil Engineering, University of Manchester, Manchester, UK, email: Meini.su@manchester.ac.uk

Abstract

Aluminium alloys are increasingly popular in structural engineering applications because they have high strength, low weight and great durability. However, the mechanical properties of aluminium alloy material may be significantly affected by high temperature. This paper presents a numerical study on the behaviour of aluminium alloy channel section columns at elevated temperatures. A non-linear finite element (FE) model was developed and validated against 27 experimental results at high temperature. The validated FE model was used to conduct an extensive parametric study, in which a total of 360 aluminium alloy channel section columns were generated at elevated temperatures. The key parameters for the parametric study include two types of aluminium alloys (6061-T6 and 6063-T5), three lengths (360mm, 1000mm and 2000mm) of columns and ten temperatures (range from 24°C to 600°C). The design strengths were calculated using American, Australia/New Zealand and European Standards and compared with the numerical results generated from parametric study. In addition, a reliability analysis was used to assess the reliability level of the considered design methods.

Keywords: Aluminium alloy; Channel section; Column; Elevated temperatures; Numerical investigation; Structural design

1. Introduction

Because of the high strength-to-weight ratio, excellent durability and great anti-corrosion properties, aluminium alloys are widely used in modern structures. The design specifications for aluminium alloy structures, such as the American Aluminium Design Manual (AA) [1], the Australia and New Zealand Standard (AS/NZS) [2], the Eurocode 9 (EC9) [3, 4] and the Chinese Standard (CN) [5], have been published.

Fire is one of the most common, dangerous and destructive disasters that structures may encounter during their service life. However, the high temperature properties of aluminium alloys differ from those at room temperature. High temperature significantly affects their mechanical properties due to the low melting point (i.e. around 650°C). For instance, the yield strength of alloy 6061-T6 at 450°C decreases to less than 53% compared to that at room temperature [6]. The diminished material properties greatly affect the structural performance of the components. It is significant and necessary to investigate the strength and failure mode of members under elevated temperature conditions, because existing researches on aluminium alloy structures at room temperature cannot be directly applied to the fire design. Since the thermal expansion in aluminium alloys is higher than that of carbon steel, it implies that the thermal strains developed in aluminium alloys would be greater, which would result in larger thermal stresses when members are thermally restrained [7]. For a uniformly heated column without thermal restraint, the effect of heating would result in member elongation. However, the presence of thermal restraint would inhibit the elongation of a compressed member, resulting in development of additional compressive stresses/forces in the member and could result in early failure of the compressed member.

There have been considerable investigations regarding to aluminium alloy columns at room temperature. Zhu and Young [8, 9] presented test results of aluminium alloy square, rectangular and circular hollow section (SHS, RHS, and CHS, respectively) columns and assessed the accuracy of design rules in the existing specifications. It is shown that the column design strengths predicted by the American, Australian/New Zealand and European specifications are generally conservative. Su et al. [10] carried out a number of stub column experiments on aluminium alloy box sections and found that the continuous strength method (CSM) offered improved design capacities. Wang and Fan [11] presented tests on the stability of aluminium alloy 6082-T6 columns and compared the test strengths with the strength predictions. It found that the AA and EC9 predictions are generally conservative especially for columns with small slenderness ratios, and the AS/NZS predictions are unsafe for more columns. Liu et al. [12] studied the buckling behaviours of complicated section aluminium alloy columns and found that the direct strength method can be more accurate and convenient to predict the ultimate strength of columns under axial compression. Wang et al. [13] investigated the performance of aluminium alloy I-section columns with fixed-end conditions by experiments and numerical simulations and assessed four design standards. It was shown that the design provisions in the above standards provide relatively conservative compressive strength predictions. Su and Young [14] presented tests and numerical simulations of aluminium alloy stocky hollow sections under concentrated transverse loads. These researches have established a good foundation for the study of performance of aluminium alloy members at room temperature.

In addition, some studies have focused on the material properties and structural behaviours of

aluminium alloys at high temperatures. Maljaars et al. [15, 16] performed a series of steady and transient state tests on 5083-H111 and 6060-T66 aluminium alloys columns at high temperature and provided simulations of compression tests at high temperature with a finite element (FE) model, which included SHS and angle sections (AS). Afterwards, Maljaars et al. [17] presented a new design method for aluminium columns under fire. Summers et al. [18] presented experiments to investigate the residual mechanical properties of the aluminium alloys AA5083-H116 and AA6061-T651 under fire and established an empirical formula to evaluate the residual yield strength. The evolution models of residual yield strength were established, which can estimate the residual yield strength after a complex thermal exposure, such as in a realistic fire. Jiang et al. [19] presented the experimental and numerical results of CHS and RHS columns under fire conditions and proposed formulae for aluminium alloy columns under fire conditions. It is found that the proposed formulae can provide accurate stability coefficients than existing codes. As an open section, plain and lipped channel sections have better integrity and pleasing line shape, and is easy to connect. It can be used in roof of long-span structure and supporting system of glass curtain wall. However, there is limited experimental or numerical studies on open section columns, such as channel sections, at elevated temperatures.

Therefore, this study investigated the buckling performance and design of aluminium alloy channel columns at elevated temperatures. In this study, aluminium alloy compression test results [14] and tensile coupon test results [6] at elevated temperatures were collected from the literature. A FE model of aluminium alloy column was established by ABAQUS 6.14 [20] and validated by the collected experimental results. Upon validation, the FE model was used to generate 360 numerical

89 results in the parametric study. The design specifications from American, Australia/New Zealand and
90 Europe were employed to predict the compression strengths and compared with the numerical results.
91 Finally, the reliability levels of the aforementioned design codes were evaluated by reliability analysis.
92

93 **2. Summary of the test results**

94 *2.1 Collected column test results obtained at elevated temperatures*

95 Maljaars et al. [15] reported both steady and transient state compression tests on an aluminium alloy
96 column exposed to elevated temperature. A series of 27 steady-state test results were collected and
97 used in this paper to validate the newly developed FE model. The steady-state tests were carried out
98 with a constant elevated temperature and a constant strain. In terms of the column tests, firstly,
99 specimens were exposed to a specific temperature before applying loads. The specimens tested at
100 180°C are subjected to 120°C for 180 minutes prior to testing. The specimens tested at higher
101 temperatures are subjected to 270°C for 30 minutes. Specimens were not restrained during heating.
102 Then, cooling specimen down to ambient temperature and heating of the specimen from ambient to
103 test temperature again within approximately 20 minutes. Similarly, specimens were not restrained
104 during heating. Maintain the test temperature constant for approximately 20 minutes. Finally, apply
105 loads to specimens by strain rate control at 2.5×10^{-3} /min to 7.0×10^{-3} /min. The cross-section of the
106 columns included square hollow section (SHS) and angle sections (AS). The columns were extruded
107 by the aluminium alloys 6060-T66 and 5083-H111. For alloy 6060-T66, the flat width
108 (b)-to-thickness (t) ratios b/t equal to 25, 44 and 60. For alloy 5083-H111, the b/t ratio equals 50.
109 Notably, the SHS extruded by alloy 5083-H111 was welded by two channel sections that were folded

by plates, so there were two longitudinal welds along the specimen. It has been assumed that the welding does not affect the temper or constitutive properties during the test because the plate of alloy 5083 was already in soft temper [15]. The length (L) of all specimens was 300 mm. The test temperatures ranged from 20°C to 400°C. The details of the dimensions, test setup and material properties can be found in [15]. The ultimate strengths of test columns (P_{exp}) are shown in Table 1.

2.2 Collected tensile coupon test results

This paper also collected the experimental results reported by Su and Young [6] regarding to the material properties of the aluminium alloys 6061-T6 and 6063-T5 at high temperature. The results of 15 steady-state coupon tests were collected and used in this paper. During testing, the specimen was heated to the specified temperature, and then loaded until it failed. The specimens were loaded at 10 different nominal temperatures of 24, 100, 200, 250, 300, 350, 400, 450, 500 and 600°C, respectively. During the experiment, the upper end of the specimens was clamped, and the lower end expanded freely during heating until the required temperature was reached. The temperature rate is 15°C /min. After stabilizing the required temperature for ten minutes, the lower end of the coupon specimen was clamped for tensile test. Tensile load was applied to the specimen by displacement control at 0.3 mm/min. The duration of each specimen is different, ranging from 40 minutes to 120 minutes. The material properties at high temperature are shown in Table 2 for aluminium alloy 6061-T6 and Table 3 for aluminium alloy 6063-T5. The full stress-strain curves of both alloys at elevated temperatures are presented in Ref [6].

3. Numerical study

A FE software ABAQUS [20] was used to carry out numerical modelling in this study. The developed FE model was validated by 27 steady-state compression test results [15]. Upon validation, a parametric study on the performance of aluminium alloy channel section columns at high temperatures was carried out, and 360 numerical results were generated.

3.1 Finite element modelling

A reliable and accurate non-linear FE model for aluminium alloy channel columns at room temperature was developed and validated by Zhu et al. [21]. In this paper, the FE model was revised for modelling columns at high temperature. The FE modelling comprised two steps: first, obtain the eigenvalue buckling modes of a column without imperfection by elastic buckling analysis; secondly, conduct non-linear analysis to obtain the ultimate load capacity and failure mode of column incorporated with imperfection. Two types of geometric imperfections were considered in the FE model. The magnitude of the local imperfection was taken as 10% of the element thickness, and the magnitude of the overall imperfection was chosen as 1/2000 of the column length. Zhu et al. [21] have conducted experimental studies on channel section columns at room temperature; the failure modes observed include local buckling, the interaction of local and flexural buckling, and a combination of local, flexural, and flexural-torsional buckling [1]. Distortional buckling was not observed in experiments conducted at room temperature. Therefore, the distortional mode is not considered as the initial geometric imperfection. The FE model employed the S4R shell elements. The element size of all columns was 5 mm × 5 mm. The measured cross-sectional dimensions and material

properties of specimens at high temperature, reported by Maljaars et al. [15], were incorporated in the FE model. The boundary conditions of the fixed ends were simulated by constraining the degrees of freedom of the nodes at both ends except the translational degree of freedom at one end of the column in the axial direction.

In finite element modelling, true stress-strain curves are used. In the non-linear analysis stage, material non-linearity or plasticity was included in the FE model using a mathematical model known as the incremental plasticity model, in which true stresses (σ_{true}) and true plastic strains ($\varepsilon_{\text{true}}^{\text{pl}}$) were specified. The true stresses and true plastic strains were obtained from the static engineering stresses (σ) and strains (ε) using Eqs. (1) and (2) as specified in the FE model, where E is the initial Young's modulus of the static engineering stress–strain curve.

$$\sigma_{\text{true}} = \sigma(1+\varepsilon) \tag{1}$$

$$\varepsilon_{\text{true}}^{\text{pl}} = \ln(1+\varepsilon) - \sigma_{\text{true}} / E \tag{2}$$

3.2 Model validation

The numerical results were compared to a total of 27 steady-state compression test results [15], as shown in Table 1. According to the results, the ultimate strengths obtained from the FE model were close to the ultimate loads obtained from experiments. The average value of the ultimate load ratio P_{Exp} / P_{FE} between the experiment and the FE analysis is 0.99, and the corresponding coefficient of variation (CoV) is 0.083. The comparisons of typical failure modes from the experiments and numerical simulations of the column are shown in Fig. 1. The curves of the load-displacement of typical columns from the FE model are plotted and compared with the experimental curves, as shown

in Fig. 2. The results show that the FE model could accurately predict the ultimate load capacities and loading behaviours of the test columns at high temperature. Thus, the FE model has been validated by Channel section column tests at room temperature [21] as well as SHS and Angle section column tests at elevated temperatures [15], since the Channel section column test result at elevated temperatures is not available.

3.3 Parametric study

The FE model accurately predicted the ultimate load capacities as well as the type of failure modes of columns tested by Maljaars et al. [15]. Hence, an extensive parametric study was conducted to study the influences of key parameters on the structural responses of channel section columns at elevated temperatures. The parametric study generated a total of 360 numerical results covering high-strength (6061-T6) and normal-strength (6063-T5) aluminium alloys. The material properties of these two alloys at elevated temperatures can be found in the literature [6], as shown in Tables 2-3. The parametric study considered both plain and lipped channel sections. In parametric study, the boundary conditions were set as fixed-ended. The fixed-ended boundary condition was simulated by restraining all the degrees of freedom of the nodes at both ends, except for the translational degree of freedom in the axial direction at one end of the column. The nodes other than the two ends were free to translate and rotate in any directions. The considered temperatures were 24, 100, 200, 250, 300, 350, 400, 450, 500 and 600°C, and the effective lengths included 360, 1000 and 2000 mm. There was no weld in the modelled specimens and residual stress was not incorporated because it has little effect on the extruded aluminum alloy members [22]. The dimensions of the channel sections are shown in

194 Table 4, where H, B, B_l, t are the depth of the cross section, width of the cross section, stiffener
195 length and thickness of the cross section, respectively, as shown in Fig. 3. The specimens were
196 labelled to identify the type of aluminium alloy, the type of section, the column length and the
197 temperature. For instance, the label "H-P1-L360-T100" defines the following specimen:

198 - The first part shows the type of alloy of the column. "H" indicates the aluminium alloy
199 6061-T6 and "N" indicates the aluminium alloy 6063-T5.
200 - The next part of the label shows the type of section, where "P" refers to the plain channel
201 section, and "L" refers to the lipped channel section. The detailed cross-sectional dimensions
202 of the specimen are shown in Table 4.
203 - The third part of the label shows the nominal length of the column, where "L360" means that
204 the specimen nominal length is 360 mm.
205 - The last part of the label "T100" means that the environment temperature is 100°C.

206

207 The ultimate strengths of columns at elevated temperatures from the parametric study are presented
208 in Tables 5-8 and Fig. 4, together with the classification of cross-sections and section slenderness
209 ratio (H/t, B/t). It can be concluded from the parametric study results that a significant decrease in the
210 load capacities can be observed from 300°C to 600°C for the aluminium alloy 6061-T6 columns,
211 while for the aluminium alloy 6063-T5 specimens, the reduction in ultimate strengths is generally
212 consistent from 100°C to 600°C.

213

214 The columns modelled in the parametric study showed several different failure modes (see Fig.5).
215 For plain channel section columns, the failure mode of the short column was local buckling, the

medium-long columns failed by a combination of local and flexural buckling and the long columns failed by flexural buckling. For lipped channel section columns, the short columns failed by local buckling and the medium-long columns failed by local and flexural buckling, which are similar to plain channel section columns. The failure modes of long columns included flexural bucking and flexural-torsional buckling.

4. Comparisons with the design methods

A total of 360 numerical results generated from parametric study were compared with the design strengths predicted by the AA [1], AS/NZS [2] and EC9 [4] standards.

4.1 Aluminium Design Manual

The column strength prediction at ambient temperature of the AA specification (P_{AA}) uses the lowest of the available strengths for the limit states of member buckling (P_{nc1}), local buckling (P_{nc2}), and the interaction between member buckling and local buckling (P_{nc3}). This is determined as shown in Eq. (3), while detailed calculation steps have summarized by Zhu et al. [20]:

$$P_{AA} = \min(P_{nc1}, P_{nc2}, P_{nc3}) \quad (3)$$

The AA [1] calculates the load capacity of members at high temperatures by reducing the mechanical properties of aluminium alloy obtained from ambient temperature. The reduction factor of the elasticity modulus for all 6XXX series alloys is the same, whereas the reduction factors of the yield and ultimate strengths at elevated temperatures are different for alloys 6061-T6 and 6063-T5.

The detailed reduction factor can be found in Part 1 of the AA [1]. The material properties at high temperatures reduced according to the codified factor in AA is shown in Tables 2-3. In this study, both the measured material properties by tensile coupon tests at elevated temperatures and the codified material properties in AA were used for calculation, and the corresponding design strengths were indicated by P_{AA-1} and P_{AA-2}, respectively.

4.2 Australian/New Zealand Standard

The design approach in the AS/NZS [2] ($P_{AS/NAS-1}$) is similar to the AA specification, as shown in Section 3.4.8 [2]. The material properties used for the calculation were measured at elevated temperatures, since the AS/NZS does not provide recommended material properties at high temperatures.

4.3 Eurocode 9

According to the Eurocode 9 [3], under the axial compression loading, structure members could fail by flexural, torsional or flexural torsional and local squashing. Effective cross-section method is used to calculate the compression section capacity. The design rule strength (P_{EC9}) in the Eurocode 9 [3] of compression members at room temperature is the minimum value of design resistance ($P_{c,Rd}$) and design buckling resistance ($P_{b,Rd}$), while detailed calculation steps have summarized by Zhu et al. [21]:

$$P_{EC9} = \min(P_{c,Rd}, P_{b,Rd}) \quad (4)$$

The reduction factor of the yield strengths and modulus of elasticity are shown in Chapter 3.2 of

257 Eurocode 9 [4], while the design procedure is presented in Eurocode 9 [3]. The residual material
258 properties at high temperatures were calculated and shown in Tables 2-3. The material properties
259 used for the calculation were taken as the measured material properties at high temperatures for P_{EC9-1}
260 and the measured room temperature properties multiplied by codified reduction factors for P_{EC9-2}.
261

262 *4.4 Result comparisons*

263 The ultimate strengths of the aluminium alloy channel column at elevated temperatures were
264 predicted by the AA [1], AS/NZS [2] and EC9 [3, 4] specifications. The predicted strengths were
265 compared with the numerical results obtained from the parametric study. The comparisons of the
266 results are summarised in Fig. 6, as well as Tables 9-12. In the comparison, all partial safety factors are
267 set to be the unity.
268

269 For high strength aluminium alloy columns (Series H-P and H-L), the predictions from the AA
270 standard with the measured material properties are the most accurate and consistent among all design
271 methods, i.e., the mean values of the load ratio P_{FE} / P_{AA-1} are found to be 1.00 and 1.07 with CoVs of
272 0.070 and 0.048, respectively. In terms of the AS/NZS specification predictions with measured
273 material properties, the mean values of the load ratio $P_{FE} / P_{AS/NAS-1}$ are 1.04 and 1.12 with CoVs of
274 0.104 and 0.082, respectively, which are also rather accurate. The predictions from EC9 with the
275 measured material properties are slightly conservative, i.e., the mean values of the load ratio
276 P_{FE} / P_{EC9-1} are 1.12 and 1.26 with CoVs of 0.060 and 0.089, respectively. However, the predictions of
277 AA and EC9 using the codified material properties are significantly conservative and hugely scattered,

especially after 250°C. The reason is mainly attributed to the inaccurate reduction in the material properties. The mean values of P_{FE} / P_{AA-2} for plain and lipped channel sections are up to 6.26 and 6.86 with CoVs of 1.067 and 1.049, respectively. Similarly, the mean values of the load ratio P_{FE} / P_{EC9-2} for plain and lipped channel sections are 5.48 and 6.05 with CoVs of 0.907 and 0.885, respectively. Based on the results, it is found that when using the measured material properties, all the three design standards show high accuracy and consistency with the AA being the best.

Regarding to the normal strength aluminium alloy columns (Series N-P and N-L), the accuracy and consistency of the predicted results are much higher by substituting the measured material properties at high temperature into the AA, AS/NZS and EC9 standards. When using the measured material properties, the predictions by the AA are the most accurate, i.e., the mean values of the load ratio P_{FE} / P_{AA-1} are 1.01 and 1.08 with CoVs of 0.066 and 0.049, respectively, followed by the AS/NZS and EC9. For plain channel section, EC9 provides most consistent prediction, while for lipped channel sections, the AA is more consistent than the other two standards. Similar to the high strength aluminium alloy columns, when using the codified properties of the material, the accuracy and consistency of the design strengths by the AA and EC9 are decreased - the mean values of the load ratio P_{FE} / P_{AA-2} are 3.22 and 3.48 for plain and lipped channel sections with CoVs being 0.631 and 0.621, respectively; the mean values of the load ratio P_{FE} / P_{EC9-2} for plain and lipped channel sections are 2.29 and 2.61 with CoVs of 0.472 and 0.448, respectively.

5. Reliability analyses

Reliability analyses were employed to evaluate the reliability levels of the design codes in this study. The safety level of the design method can be reasonably measured by the reliability index (β). In the AA [1], AS/NZS [2] and Eurocode 9 [3, 4], the target index β of aluminium alloy structural component design is set to be 2.5. If the derived reliability index is greater than 2.5, the design codes are considered to be safe. The design load combinations applied in the reliability analysis are 1.2D+1.6L for AA [1], 1.25D+1.5L for AS/NZS [2], 1.35D+1.5L for EC9 [3, 4], where "D" and "L" indicate the dead and live loads, respectively. The codified resistance factors (ϕ) of the AA, AS/NZS and EC9 are 0.85, 0.85 and 0.91, respectively.

The reliability index β of all design codes for the four series of specimens are shown in Tables 9-12. For high strength aluminium alloy plain channel section columns (Series H-P), the reliability indexes of the AA and EC9 using the codified material properties are found to be less than the target value of 2.50. All predicted reliability indexes of the three design methods using measured material properties are higher than the target reliability index of 2.50. For high strength aluminium alloy lipped channel section columns (Series H-L), the reliability index β of all the design codes are greater than 2.50, except for AA approach using the codified material properties. For normal strength aluminium alloy columns (Series N-P and N-L), the reliability indices of all design rules are found to be higher than the target reliability index. To summarize, when using the measured material properties at elevated temperatures, the existing design methods in the AA, AS/NZS and EC9 are rather reliable for column design at high temperatures.

6. Conclusions

This paper investigated the behaviour and design of aluminium alloy channel columns at elevated temperatures. The FE model developed by ABAQUS was validated by experimental data from Maljaars et al. [15]. The validated FE model was employed for a parametric study considering aluminium alloy columns of both plain channel and lipped channel sections at high temperatures. The parametric study generated a total of 360 numerical results. Both high and normal strength aluminium alloys (6061-T6 and 6063-T5, respectively) were considered. The material properties of the two alloys were reported by Su and Young [6] and used in this study. The temperatures considered in the study covered a wide range including 24, 100, 200, 250, 300, 350, 400, 450, 500 and 600°C. The capacities of the columns obtained by the numerical investigation were compared with the compressive strengths predicted by the existing American, Australian/New Zealand and European standards for aluminium structures. In general, the ultimate strengths predicted by the considered design methods were rather accurate when employing the measured material properties; however, the predictions could be significantly scattered and inaccurate if the codified material properties were adopted in the design. Therefore, the existing design methods for columns at ambient temperature are applicable to columns at elevated temperatures provided that accurate material properties are available and used. The reliability of the three considered standards for channel columns at elevated temperatures was assessed by reliability analysis. The results show that all the design rules using the measured material properties are reliable for the design of aluminium alloy channel columns at elevated temperatures.

Acknowledgements

The research work described in this paper was supported by the National Natural Science Foundation China (51778370, 51538007), the Key Project of Department of Education of Guangdong Province (2017B030311004) and the Shenzhen science and technology project (JCYJ20170818094820689).

Notations

b	flat width
B	section width
B_l	stiffener length of section
E_T	Young's modulus at elevated temperature
$f_{u,T}$	ultimate stress at elevated temperature
$f_{y,T}$	0.2% proof stress at elevated temperature
H	section depth
L	column length
P_{AA}	design strengths from AA standard at ambient temperature
P_{AA-1}	design strengths from AA standard using measured material properties
P_{AA-2}	design strengths from AA standard using codified material properties
$P_{AS/NZS-1}$	design strengths by the AS/NZS using measured material properties
$P_{b,Rd}$	design buckling resistance of the compression member by the EC9
$P_{c,Rd}$	design resistance to normal forces of the cross-section for uniform compression by the EC9
P_{EC9}	design strengths from EC9 at ambient temperature
P_{EC9-1}	design strengths from EC9 using measured material properties
P_{EC9-2}	design strengths from EC9 using codified material properties

364 P_{FE} ultimate loads obtained from the FE model

365 P_{nc1} member buckling strength from AA

366 P_{nc2} local buckling strength from AA

367 P_{nc3} interaction between member buckling and local buckling from AA

368 P_u experimental ultimate loads

369 t thickness of the section

370 β reliability index

371 ϕ resistance factor

References

[1] Aluminium Association, Aluminium Design Manual, The Aluminium Association, Washington, DC, 2015.

[2] AS/NZS, Aluminium Structures–Part 1: Limit State Design, Australian/New Zealand Standard AS/NZS1664.1:1997. Sydney, Australia: Standards Australia,1997

[3] European Committee for Standardization (EC9), EUROCODE 9: Design of Aluminium Structures—Part 1-1: General Rules and Rules for Buildings, BS EN 1999-1-1:2007, CEN, 2007.

[4] European Committee for Standardization (EC9), EUROCODE 9: Design of Aluminium Structures—Part 1-2: Structural fire design, BS EN 1999-1-2:2007, CEN, 2007.

[5] CN. Code for design of aluminium structures. Ministry of Construction of the People's Republic of China. GB50429-2007.

[6] Su, M. N., Young B., "Material Properties of Normal and High Strength Aluminium Alloys at Elevated Temperatures". Thin-walled Structures, in press.

[7] Neves I C, Valente J C, Rodrigues J P C. Thermal restraint and fire resistance of columns. Fire Safety Journal, 2002, 37(8):753-771.

[8] Zhu, J.H., Young, B. "Tests and Design of Aluminum Alloy Compression Members", J. Struct. Eng. ASCE 132 (7) (2006) 1096-1107.

[9] Zhu J H, Young B. "Experimental investigation of Aluminum Circular Hollow Section Columns". Engineering Structures, 2006,28(2):207~215

[10] Su M N, Young B, Gardner L. "Testing and Design of Aluminum Alloy Cross Sections in Compression". Journal of Structural Engineering, 2014, 140(9):04014047.

[11] Wang Y, Fan F, Lin S. "Experimental investigation on the stability of aluminium alloy 6082

394 circular tubes in axial compression". Thin-Walled Structures, 2015, 89:54-66.
395 [12] Liu M, Zhang L, Wang P, et al. "Buckling behaviors of section aluminum alloy columns under
396 axial compression". Engineering Structures, 2015, 95:127-137.
397 [13] Wang Y Q, Yuan H X, Chang T, et al. "Compressive buckling strength of extruded aluminium
398 alloy I-section columns with fixed-pinned end conditions". Thin-Walled Structures, 2017,
399 119:396-403.
400 [14] Su M N, Young B. "Design of aluminium alloy stocky hollow sections subjected to concentrated
401 transverse loads". Thin-Walled Structures, 2018, 124:546-557.
402 [15] Maljaars J, Soetens F, Snijder H H. "Local buckling of aluminium structures exposed to fire. Part
403 1: Tests". Thin-Walled Structures, 2009, 47(11):1404-1417.
404 [16] Maljaars J, Soetens F, Snijder H H. "Local buckling of aluminium structures exposed to fire: Part
405 2: Finite element models". Steel Construction, 2009, 47(11):1418-1428.
406 [17] Maljaars J J, Twilt L L, Soetens F F. "Flexural buckling of fire exposed aluminium columns". Fire
407 Safety Journal, 2009, 44(5):711-717.
408 [18] Summers P T, Case S W, Lattimer B Y. "Residual mechanical properties of aluminum alloys
409 AA5083-H116 and AA6061-T651 after fire". Engineering Structures, 2014, 76:49-61.
410 [19] Jiang S, Xiong Z, Guo X, et al. "Buckling behaviour of aluminium alloy columns under fire
411 conditions". Thin-Walled Structures, 2018, 124:523-537.
412 [20] ABAQUS Analysis User's Manual, version 6.14, ABAQUS Inc., 2014.
413 [21] Zhu, J.H., Li, Z, Q., Su, M.N., Young, B., "Behaviour of Aluminium Alloys Plain and Lipped
414 Channel Columns", Thin-Walled Structures, 2019, 135:306-316.
415 [21] Mazzolani FM. Aluminium alloy structures. 2nd ed. E&FN Spon Press;1995

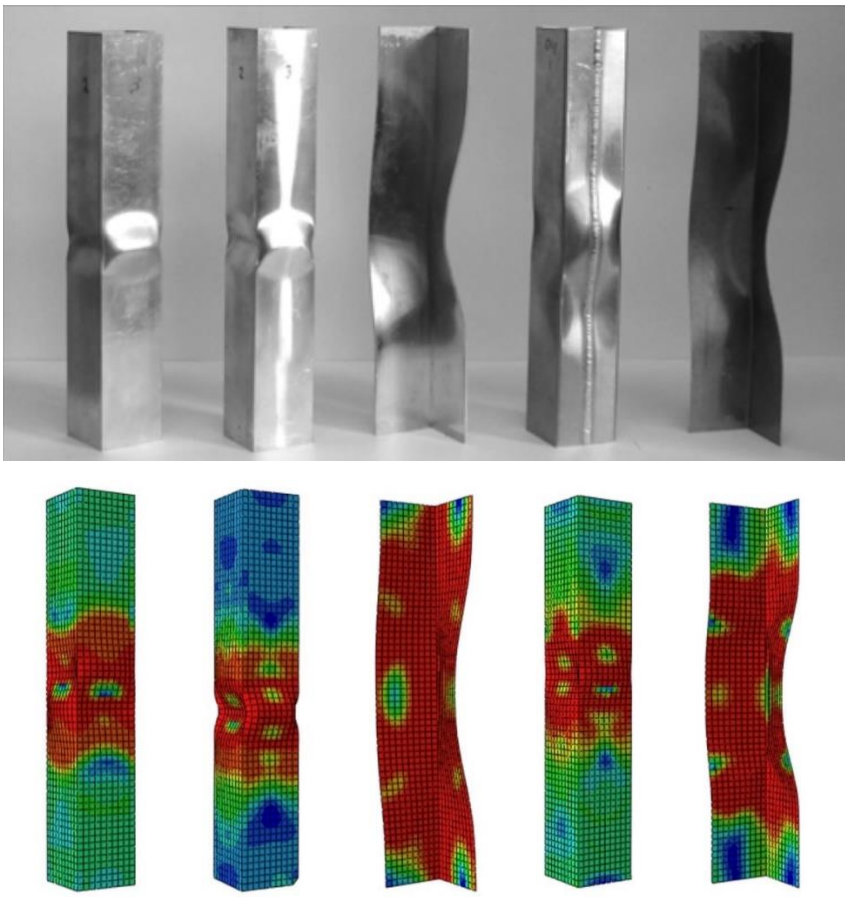

(a) 1-2 (b) T9-1 (c) TA7 (d) O6 (e) OA3

Fig.1. Typical failure modes of the test specimens and the FE models

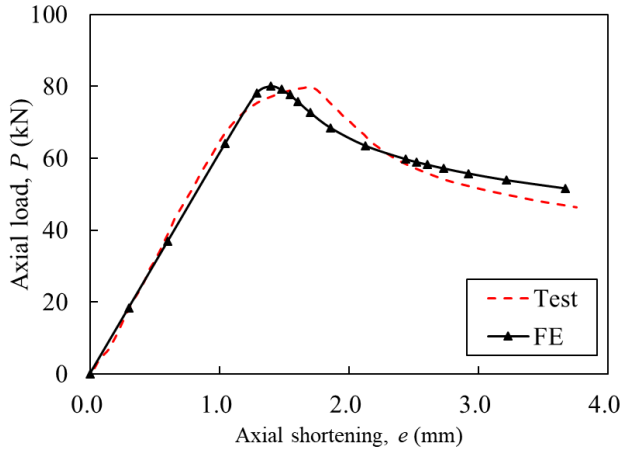

(a) Specimen 2-2

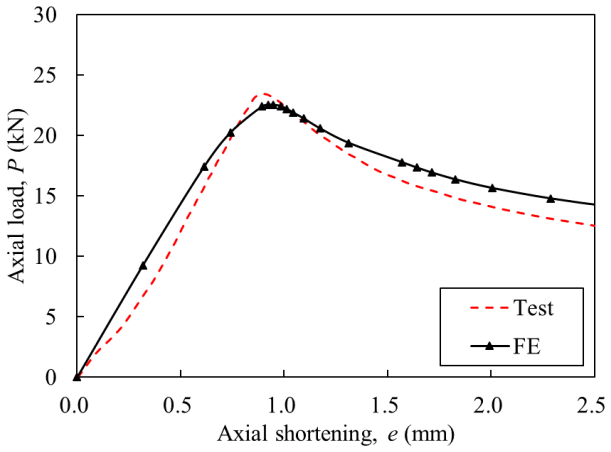

(b) Specimen T4-1

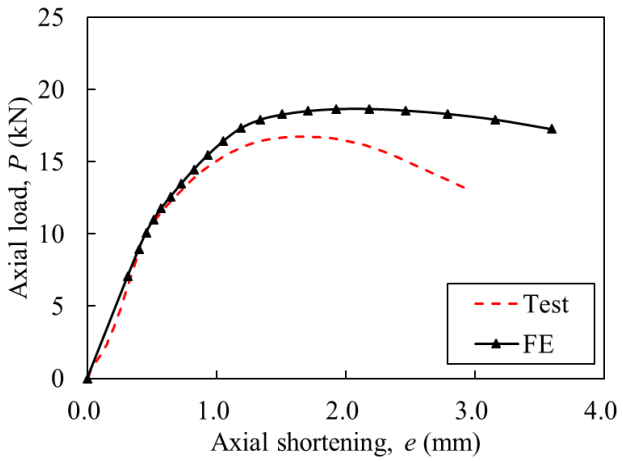

(c) Specimen TA11

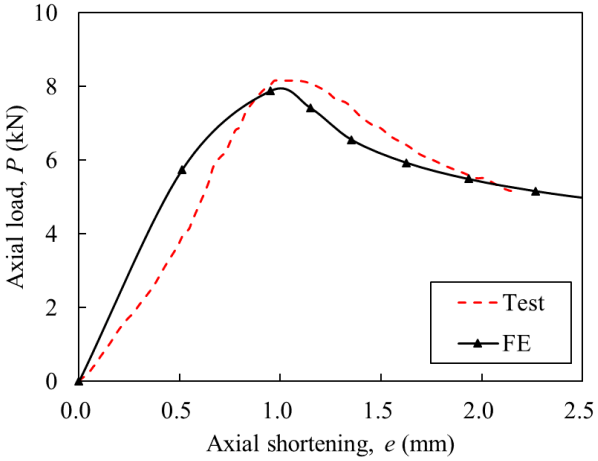

(d) Specimen O3

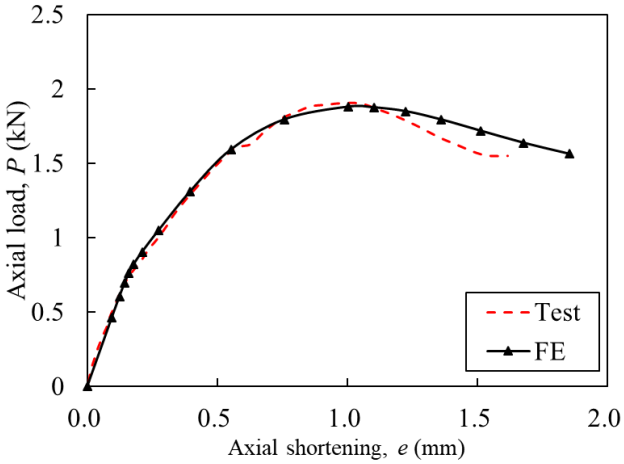

(e) Specimen OA6

Fig. 2. Comparisons of the experimental and numerical load-deformation curves

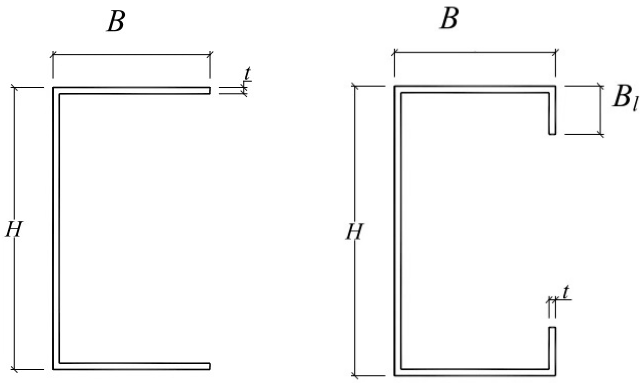

Fig. 3. Definition of symbols for cross-sections

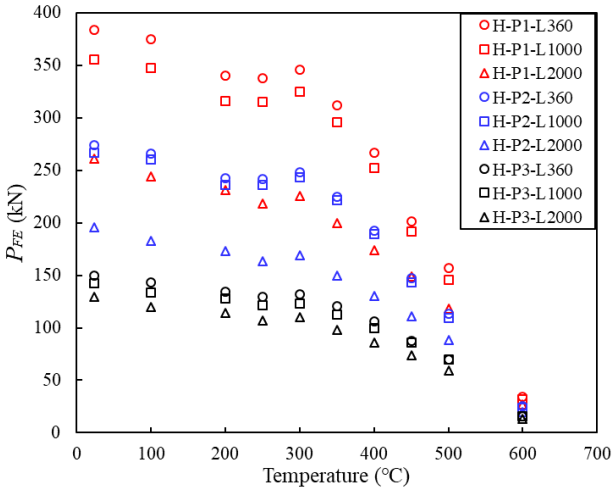

(a) Series H-P

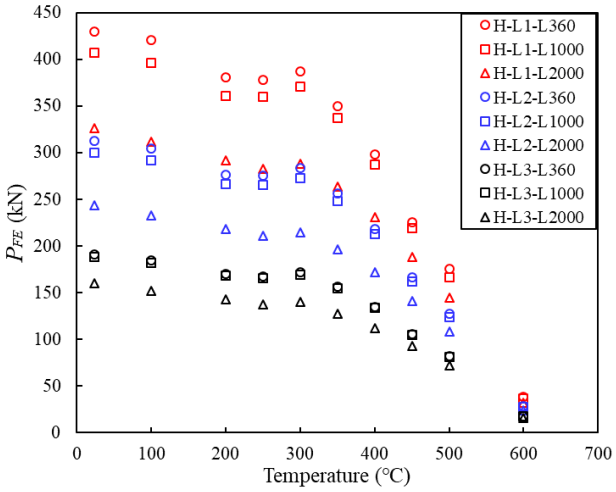

(b) Series H-L

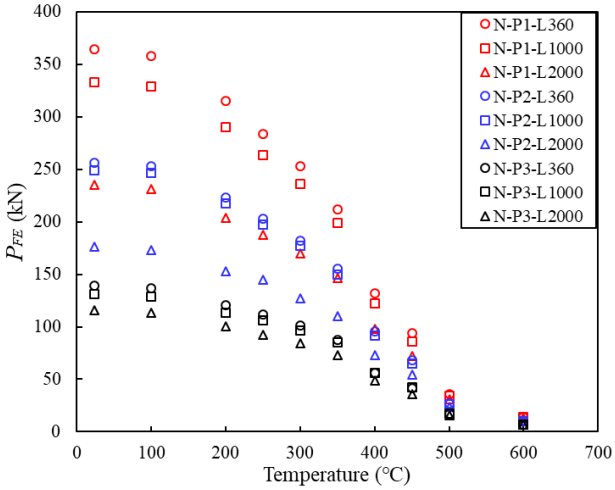

(c) Series N-P

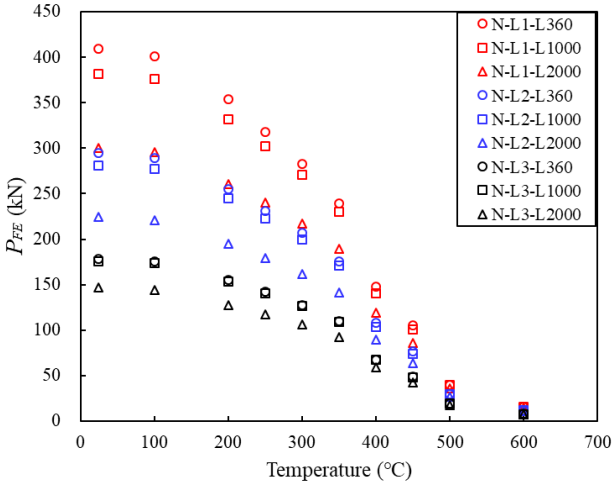

(d) Series N-L

Fig. 4. Numerical ultimate strengths of FE model at elevated temperatures

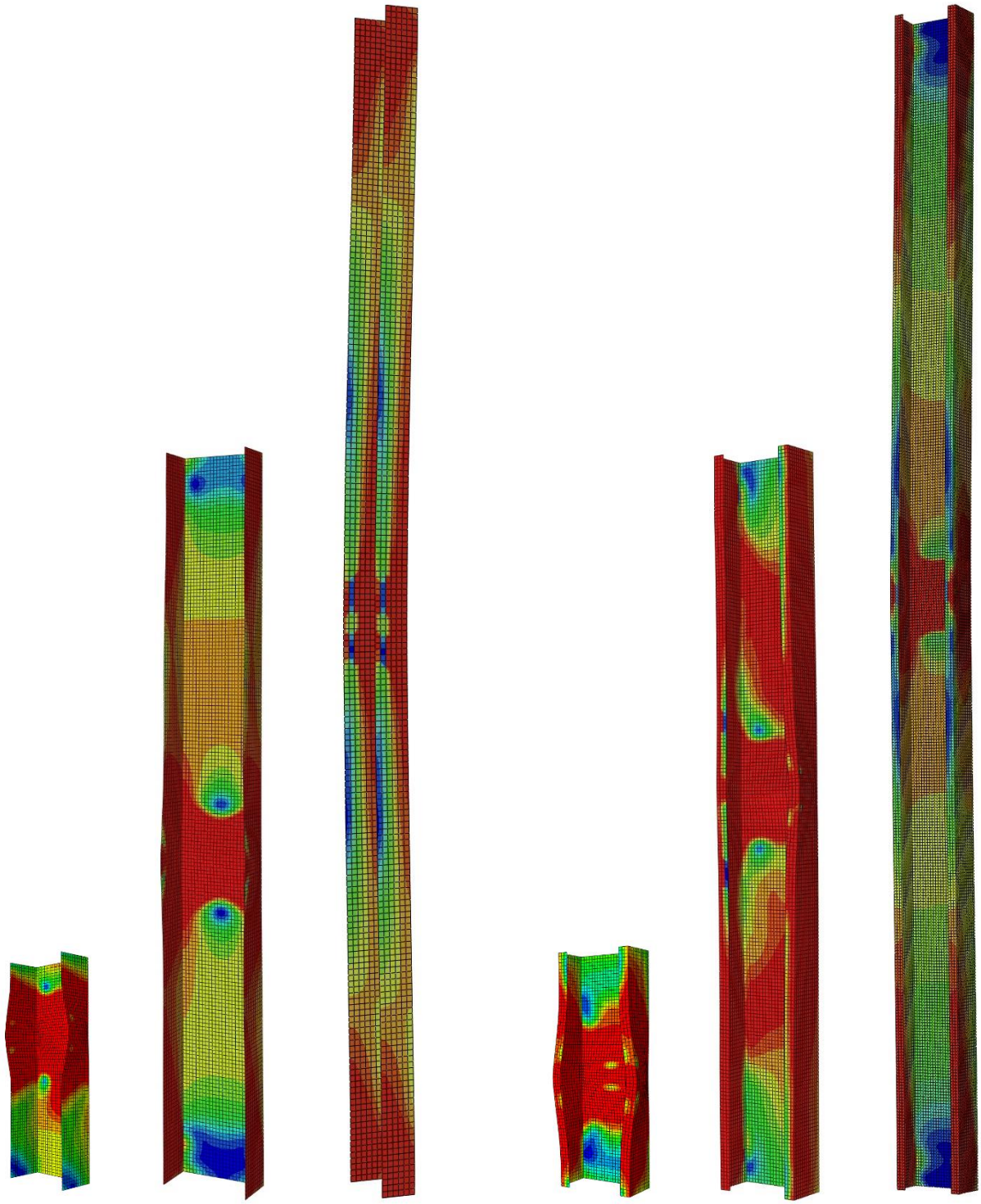

(a) (b) (c) (d) (e) (f)

[i] plain channel section [ii] lipped channel section

Fig. 5. Failure modes of specimens in the parametric study. (a) H-P2-L360-T300 (b) H-P2-L1000-T300 (c) H-P2-L2000-T300 (d) H-L2-L360-T300 (e) H-L2-L1000-T300 (f) H-L3-L2000-T300

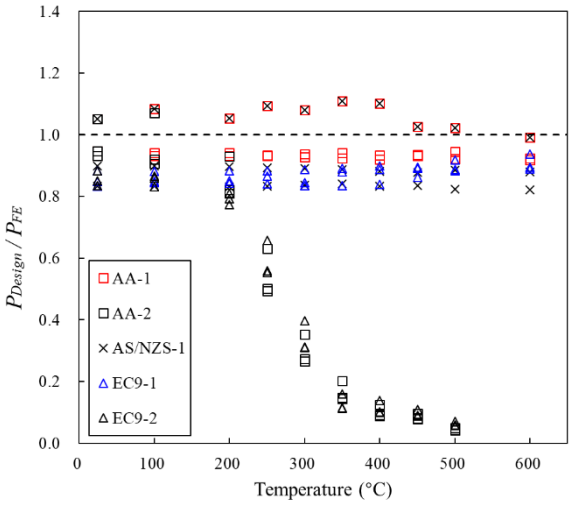

(a) Series H-P1

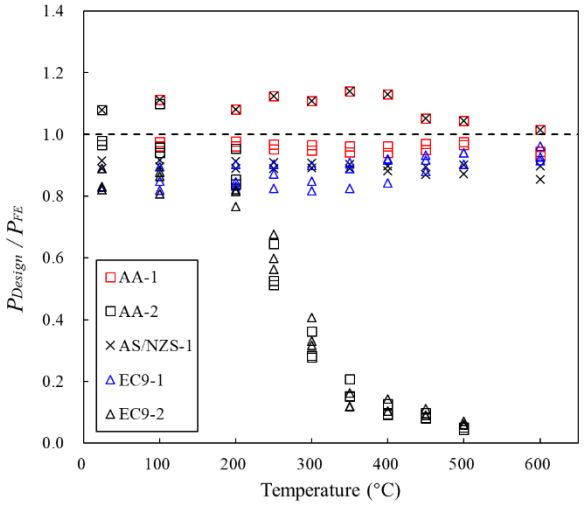

(b) Series H-P2

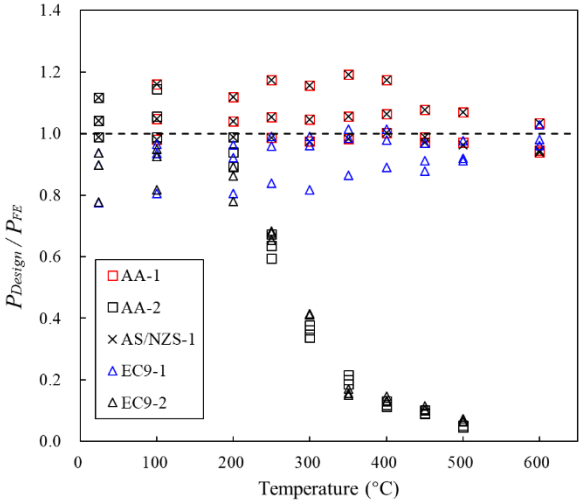

(c) Series H-P3

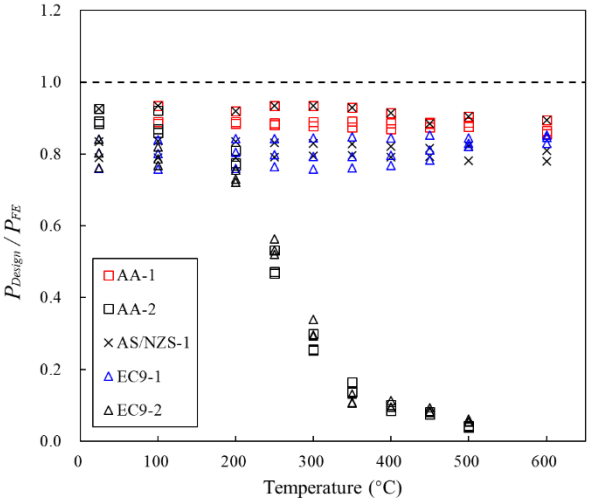

(d) Series H-L1

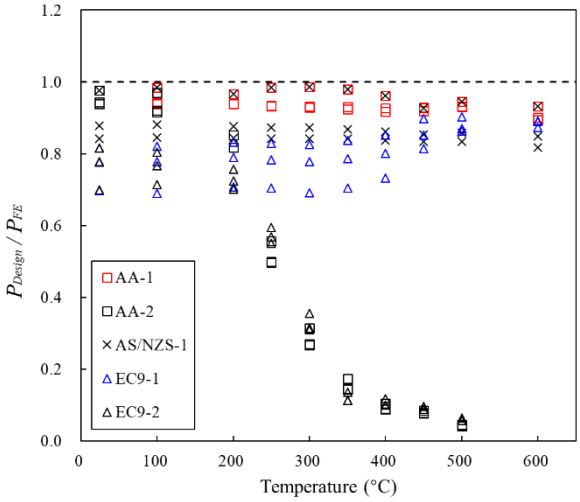

(e) Series H-L2

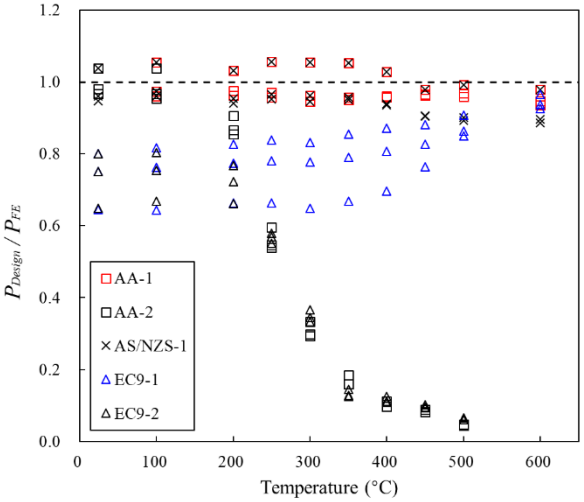

(f) Series H-L3

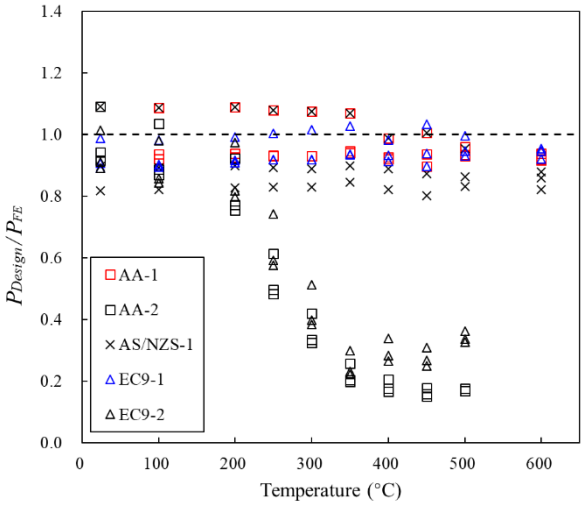

(g) Series N-P1

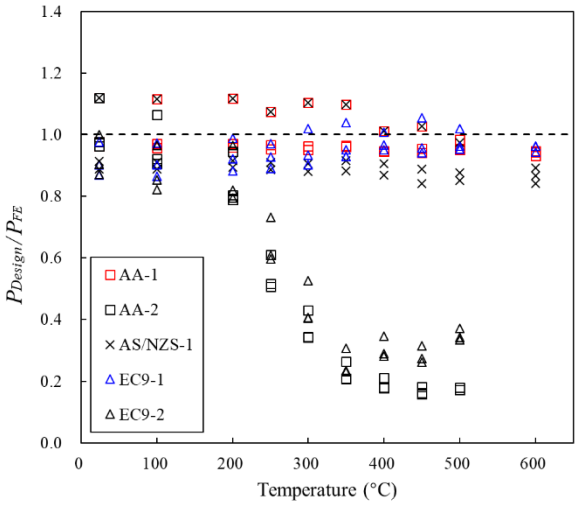

(h) Series N-P2

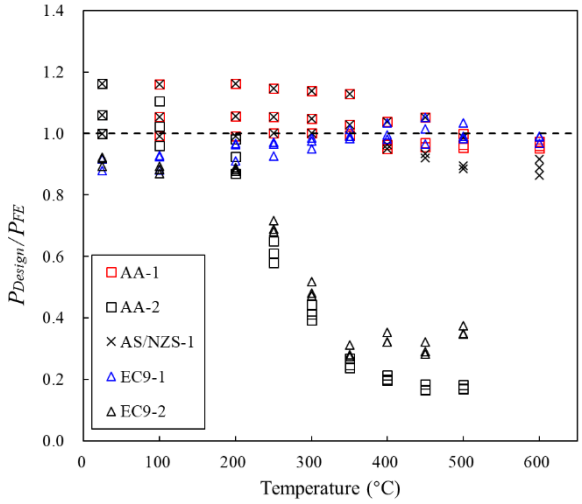

(i) Series N-P3

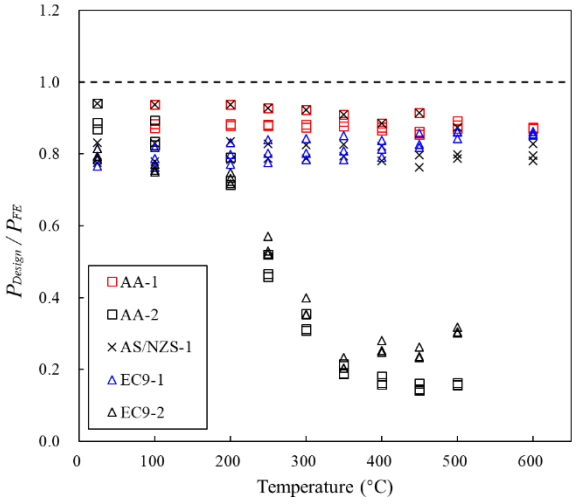

(j) Series N-L1

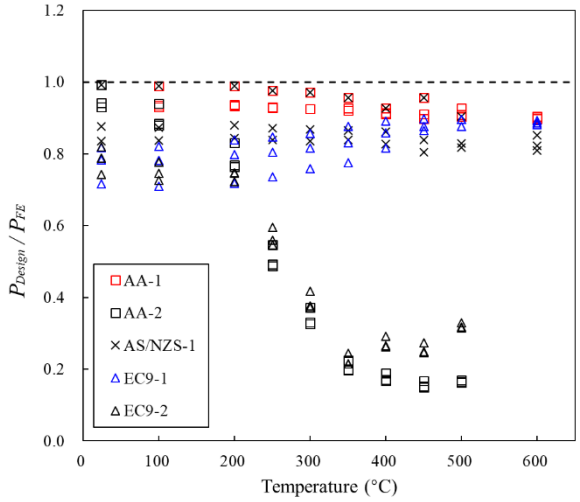

(k) Series N-L2

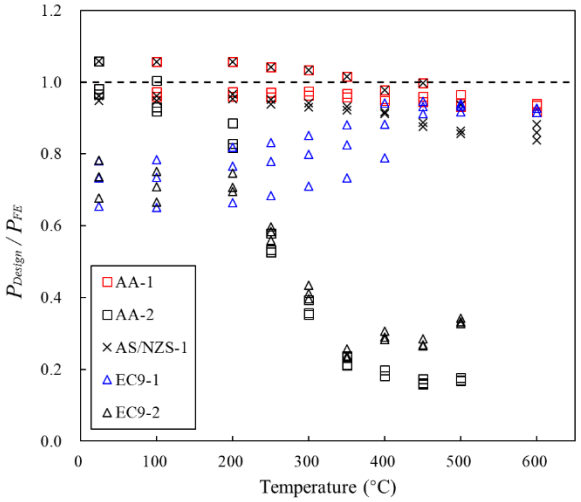

(l) Series N-L3

Fig. 6. Comparison of the design predictions with numerical ultimate strengths

456 Table. 1. Comparison of test results [15] and FE results

Specimens	Type of Cross-section	Type of Material	b (mm)	t (mm)	Test Temperature (°C)	P_{Exp} (kN)	P_{FE} (kN)	P_{Exp} / P_{FE}
1-2	SHS	6060-T66	50	2	20	78.8	80.3	0.98
2-2	SHS	6060-T66	50	2	20	79.1	80.0	0.99
T4-2	SHS	6060-T66	50	2	20	81.0	84.3	0.96
T5-2	SH	6060-T66	50	2	179	65.8	58.7	1.12
T3-2	SHS	6060-T66	50	2	265	28.8	27.1	1.06
T2-2	SHS	6060-T66	50	2	290	22.7	22.6	1.00
T9-1	SHS	6060-T66	48.2	1.1	20	26.8	29.2	0.92
T4-1	SHS	6060-T66	48.2	1.1	179	23.4	22.5	1.04
T2-1	SHS	6060-T66	48.2	1.1	268	13.1	12.3	1.07
T7-1	SHS	6060-T66	48.2	1.1	289	10.7	10.6	1.01
T1-1	SHS	6060-T66	48.2	1.1	287	11.9	10.7	1.11
1-08	SHS	6060-T66	47.6	0.8	20	12.0	13.9	0.86
2-08	SHS	6060-T66	47.6	0.8	20	11.4	13.3	0.86
TA7	AS	6060-T66	50	2	20	19.9	22.9	0.87
TA11	AS	6060-T66	50	2	171	16.8	18.6	0.90
TA4	AS	6060-T66	50	2	267	8.4	9.0	0.94
TA6	AS	6060-T66	50	2	299	7.1	7.7	0.92
O6	SHS	5083-H111	50	1	20	19.8	20.8	0.95
O9	SHS	5083-H111	50	1	178	17.9	16.3	1.10
O4	SHS	5083-H111	50	1	267	12.0	11.4	1.05
O3	SHS	5083-H111	50	1	323	8.2	7.9	1.04
O5	SHS	5083-H111	50	1	345	6.2	5.6	1.11
OA3	AS	5083-H111	50	1	20	5.1	5.9	0.86
OA4	AS	5083-H111	50	1	167	4.9	4.8	1.02
OA5	AS	5083-H111	50	1	270	2.9	3.2	0.92
OA6	AS	5083-H111	50	1	325	1.9	1.9	1.00
OA7	AS	5083-H111	50	1	339	1.5	1.6	0.94
							Mean, P_m	0.99
							CoV, V_P	0.083

457

458 Table. 2. Material properties of aluminium alloy 6061-T6 at elevated temperatures

Temperature (°C)	Su and Young [6]			AA [1]			EC9 [4]	
	E_T (GPa)	$f_{y,T}$ (MPa)	$f_{u,T}$ (MPa)	E_T (GPa)	$f_{y,T}$ (MPa)	$f_{u,T}$ (MPa)	E_T (GPa)	$f_{y,T}$ (MPa)
24	69.5	199.9	232.3	69.5	199.9	232.3	70.0	199.9
100	64.0	195.2	225.1	66.7	189.9	204.8	69.3	189.9
200	63.4	176.9	197.8	60.8	153.8	136.3	67.9	157.9
250	59.4	176.0	190.8	56.6	92.8	85.2	65.1	109.9
300	58.5	181.0	189.1	50.1	51.4	48.6	60.2	62.0
350	55.1	164.0	169.6	42.4	25.1	21.3	54.6	20.0
400	52.1	139.0	145.9	32.2	13.2	9.6	47.6	15.0
450	54.2	105.1	108.4	20.5	8.8	4.6	37.8	10.0
500	43.1	80.7	85.1	8.7	3.6	1.5	28.0	5.0
600	15.7	17.5	20.6	-	-	-	-	-

459

460

461 Table. 3. Material properties of aluminium alloy 6063-T5 at elevated temperatures

Temperature (°C)	Su and Young [6]			AA [1]			EC9 [4]	
	E_T (GPa)	$f_{y,T}$ (MPa)	$f_{u,T}$ (MPa)	E_T (GPa)	$f_{y,T}$ (MPa)	$f_{u,T}$ (MPa)	E_T (GPa)	$f_{y,T}$ (MPa)
24	65.6	186.6	226.8	65.6	186.6	226.8	70.0	186.6
100	63.4	183.7	217.6	63.0	173.5	198.0	69.3	171.7
200	56.1	163.1	183.4	57.4	132.7	121.2	67.9	141.8
250	54.2	147.1	159.3	53.4	76.5	67.4	65.1	91.4
300	51.7	131.2	138.5	47.3	45.8	34.8	60.2	54.1
350	47.3	111.9	114.2	40.0	23.5	14.1	54.6	26.1
400	33.7	67.9	71	30.4	12.3	4.7	47.6	19.6
450	44.0	47	50.6	19.4	7.9	2.1	37.8	13.1
500	34.1	18.6	19.1	8.2	3.4	0.3	28.0	6.5
600	28.9	7.3	7.6	-	-	-	-	-

462

463

464 Table. 4. Dimensions of cross-sections in parametric study

Series	H (mm)	B (mm)	B_l (mm)	t (mm)
P1	120	60	-	8
P2	120	60	-	6
P3	120	60	-	4
L1	120	60	15	8
L2	120	60	15	6
L3	120	60	15	4

465

466 Table.5. Numerical ultimate strengths of FE model at elevated temperatures of Series H-P

Specimen (H/t=15, B/t=8)	Classification of cross-sections	P_{FE}(kN)	Specimen (H/t=20, B/t=10)	Classification of cross-sections	P_{FE}(kN)	Specimen (H/t=30, B/t=15)	Classification of cross-sections	P_{FE}(kN)
H-P1-L360-T24	Class2	384.1	H-P2-L360-T24	Class3	274.2	H-P3-L360-T24	Class4	150.0
H-P1-L360-T100	Class2	375.2	H-P2-L360-T100	Class3	266.0	H-P3-L360-T100	Class4	143.0
H-P1-L360-T200	Class2	340.3	H-P2-L360-T200	Class2	242.6	H-P3-L360-T200	Class4	134.4
H-P1-L360-T250	Class2	337.6	H-P2-L360-T250	Class2	241.4	H-P3-L360-T250	Class4	129.8
H-P1-L360-T300	Class2	345.7	H-P2-L360-T300	Class3	247.9	H-P3-L360-T300	Class4	132.2
H-P1-L360-T350	Class2	312.2	H-P2-L360-T350	Class2	225.2	H-P3-L360-T350	Class4	120.8
H-P1-L360-T400	Class1	266.6	H-P2-L360-T400	Class2	192.3	H-P3-L360-T400	Class3	105.9
H-P1-L360-T450	Class1	201.2	H-P2-L360-T450	Class2	147.6	H-P3-L360-T450	Class3	87.8
H-P1-L360-T500	Class1	156.8	H-P2-L360-T500	Class1	113.0	H-P3-L360-T500	Class3	69.5
H-P1-L360-T600	Class1	34.1	H-P2-L360-T600	Class1	25.0	H-P3-L360-T600	Class1	15.3
H-P1-L1000-T24	Class2	356.0	H-P2-L1000-T24	Class3	266.6	H-P3-L1000-T24	Class4	142.4
H-P1-L1000-T100	Class2	347.4	H-P2-L1000-T100	Class3	260.1	H-P3-L1000-T100	Class4	133.9
H-P1-L1000-T200	Class2	315.7	H-P2-L1000-T200	Class2	236.4	H-P3-L1000-T200	Class4	127.6
H-P1-L1000-T250	Class2	315.6	H-P2-L1000-T250	Class2	236.3	H-P3-L1000-T250	Class4	121.6
H-P1-L1000-T300	Class2	325.0	H-P2-L1000-T300	Class3	243.5	H-P3-L1000-T300	Class4	123.2
H-P1-L1000-T350	Class2	295.8	H-P2-L1000-T350	Class2	221.6	H-P3-L1000-T350	Class4	112.5
H-P1-L1000-T400	Class1	252.4	H-P2-L1000-T400	Class2	189.0	H-P3-L1000-T400	Class3	99.8
H-P1-L1000-T450	Class1	191.4	H-P2-L1000-T450	Class2	143.4	H-P3-L1000-T450	Class3	86.2
H-P1-L1000-T500	Class1	145.8	H-P2-L1000-T500	Class1	109.2	H-P3-L1000-T500	Class3	69.5
H-P1-L1000-T600	Class1	31.8	H-P2-L1000-T600	Class1	23.8	H-P3-L1000-T600	Class1	15.4
H-P1-L2000-T24	Class2	261.4	H-P2-L2000-T24	Class3	195.7	H-P3-L2000-T24	Class4	129.1
H-P1-L2000-T100	Class2	244.1	H-P2-L2000-T100	Class3	182.6	H-P3-L2000-T100	Class4	119.8
H-P1-L2000-T200	Class2	231.5	H-P2-L2000-T200	Class2	173.2	H-P3-L2000-T200	Class4	114.2
H-P1-L2000-T250	Class2	218.6	H-P2-L2000-T250	Class2	163.4	H-P3-L2000-T250	Class4	107.0
H-P1-L2000-T300	Class2	225.8	H-P2-L2000-T300	Class3	168.9	H-P3-L2000-T300	Class4	110.5
H-P1-L2000-T350	Class2	200.1	H-P2-L2000-T350	Class2	149.7	H-P3-L2000-T350	Class4	97.8
H-P1-L2000-T400	Class1	174.0	H-P2-L2000-T400	Class2	130.2	H-P3-L2000-T400	Class3	85.6
H-P1-L2000-T450	Class1	148.6	H-P2-L2000-T450	Class2	111.2	H-P3-L2000-T450	Class3	74.0
H-P1-L2000-T500	Class1	118.1	H-P2-L2000-T500	Class1	88.5	H-P3-L2000-T500	Class3	58.9
H-P1-L2000-T600	Class1	26.6	H-P2-L2000-T600	Class1	19.9	H-P3-L2000-T600	Class1	13.3

467

468 Table.6. Numerical ultimate strengths of FE model at elevated temperatures of Series H-L

Specimen (H/t=15, B/t=8)	Classification of cross-sections	P_{FE}(kN)	Specimen (H/t=20, B/t=10)	Classification of cross-sections	P_{FE}(kN)	Specimen (H/t=30, B/t=15)	Classification of cross-sections	P_{FE}(kN)
H-L1-L360-T24	Class2	430.5	H-L2-L360-T24	Class3	312.9	H-L3-L360-T24	Class4	191.4
H-L1-L360-T100	Class2	420.6	H-L2-L360-T100	Class3	304.3	H-L3-L360-T100	Class4	184.4
H-L1-L360-T200	Class2	381.1	H-L2-L360-T200	Class2	276.2	H-L3-L360-T200	Class4	170.5
H-L1-L360-T250	Class2	378.6	H-L2-L360-T250	Class2	275.6	H-L3-L360-T250	Class4	167.5
H-L1-L360-T300	Class2	387.7	H-L2-L360-T300	Class3	283.4	H-L3-L360-T300	Class4	171.9
H-L1-L360-T350	Class2	350.5	H-L2-L360-T350	Class2	256.8	H-L3-L360-T350	Class4	156.3
H-L1-L360-T400	Class1	298.7	H-L2-L360-T400	Class2	218.8	H-L3-L360-T400	Class3	134.7
H-L1-L360-T450	Class1	225.4	H-L2-L360-T450	Class2	166.2	H-L3-L360-T450	Class3	105.5
H-L1-L360-T500	Class1	175.6	H-L2-L360-T500	Class1	127.5	H-L3-L360-T500	Class3	82.0
H-L1-L360-T600	Class1	38.2	H-L2-L360-T600	Class1	28.2	H-L3-L360-T600	Class1	17.9
H-L1-L1000-T24	Class2	407.6	H-L2-L1000-T24	Class3	300.1	H-L3-L1000-T24	Class4	188.7
H-L1-L1000-T100	Class2	396.8	H-L2-L1000-T100	Class3	292.1	H-L3-L1000-T100	Class4	181.7
H-L1-L1000-T200	Class2	360.7	H-L2-L1000-T200	Class2	266.2	H-L3-L1000-T200	Class4	168.1
H-L1-L1000-T250	Class2	360.3	H-L2-L1000-T250	Class2	265.5	H-L3-L1000-T250	Class4	165.3
H-L1-L1000-T300	Class2	370.9	H-L2-L1000-T300	Class3	273.3	H-L3-L1000-T300	Class4	169.1
H-L1-L1000-T350	Class2	337.2	H-L2-L1000-T350	Class2	248.8	H-L3-L1000-T350	Class4	155.2
H-L1-L1000-T400	Class1	287.8	H-L2-L1000-T400	Class2	212.7	H-L3-L1000-T400	Class3	134.2
H-L1-L1000-T450	Class1	219.1	H-L2-L1000-T450	Class2	162.3	H-L3-L1000-T450	Class3	105.2
H-L1-L1000-T500	Class1	166.9	H-L2-L1000-T500	Class1	123.9	H-L3-L1000-T500	Class3	81.2
H-L1-L1000-T600	Class1	36.8	H-L2-L1000-T600	Class1	27.2	H-L3-L1000-T600	Class1	17.7
H-L1-L2000-T24	Class2	326.9	H-L2-L2000-T24	Class3	244.2	H-L3-L2000-T24	Class4	160.1
H-L1-L2000-T100	Class2	312.3	H-L2-L2000-T100	Class3	233.3	H-L3-L2000-T100	Class4	152.2
H-L1-L2000-T200	Class2	292.0	H-L2-L2000-T200	Class2	218.1	H-L3-L2000-T200	Class4	142.8
H-L1-L2000-T250	Class2	282.5	H-L2-L2000-T250	Class2	210.7	H-L3-L2000-T250	Class4	137.2
H-L1-L2000-T300	Class2	288.1	H-L2-L2000-T300	Class3	214.8	H-L3-L2000-T300	Class4	140.2
H-L1-L2000-T350	Class2	263.7	H-L2-L2000-T350	Class2	196.7	H-L3-L2000-T350	Class4	127.8
H-L1-L2000-T400	Class1	230.7	H-L2-L2000-T400	Class2	172.2	H-L3-L2000-T400	Class3	112.3
H-L1-L2000-T450	Class1	188.3	H-L2-L2000-T450	Class2	140.8	H-L3-L2000-T450	Class3	92.8
H-L1-L2000-T500	Class1	145.2	H-L2-L2000-T500	Class1	108.7	H-L3-L2000-T500	Class3	71.9
H-L1-L2000-T600	Class1	31.9	H-L2-L2000-T600	Class1	23.9	H-L3-L2000-T600	Class1	15.8

469

470 Table.7. Numerical ultimate strengths of FE model at elevated temperatures of Series N-P

Specimen (H/t=15, B/t=8)	Classification of cross-sections	P_{FE}(kN)	Specimen (H/t=20, B/t=10)	Classification of cross-sections	P_{FE}(kN)	Specimen (H/t=30, B/t=15)	Classification of cross-sections	P_{FE}(kN)
N-P1-L360-T24	Class1	364.9	N-P2-L360-T24	Class3	256.6	N-P3-L360-T24	Class4	139.1
N-P1-L360-T100	Class1	357.8	N-P2-L360-T100	Class3	252.9	N-P3-L360-T100	Class4	136.6
N-P1-L360-T200	Class1	315.5	N-P2-L360-T200	Class2	223.0	N-P3-L360-T200	Class4	120.6
N-P1-L360-T250	Class1	283.5	N-P2-L360-T250	Class2	202.9	N-P3-L360-T250	Class4	111.4
N-P1-L360-T300	Class1	252.9	N-P2-L360-T300	Class2	182.0	N-P3-L360-T300	Class3	101.4
N-P1-L360-T350	Class1	211.8	N-P2-L360-T350	Class1	155.0	N-P3-L360-T350	Class3	87.8
N-P1-L360-T400	Class1	132.3	N-P2-L360-T400	Class1	95.4	N-P3-L360-T400	Class2	56.4
N-P1-L360-T450	Class1	93.9	N-P2-L360-T450	Class1	68.3	N-P3-L360-T450	Class1	41.7
N-P1-L360-T500	Class1	35.8	N-P2-L360-T500	Class1	26.7	N-P3-L360-T500	Class1	17.4
N-P1-L360-T600	Class1	14.2	N-P2-L360-T600	Class1	10.6	N-P3-L360-T600	Class1	7.0
N-P1-L1000-T24	Class1	333.0	N-P2-L1000-T24	Class3	249.3	N-P3-L1000-T24	Class4	131.1
N-P1-L1000-T100	Class1	329.1	N-P2-L1000-T100	Class3	246.5	N-P3-L1000-T100	Class4	128.3
N-P1-L1000-T200	Class1	290.3	N-P2-L1000-T200	Class2	217.4	N-P3-L1000-T200	Class4	113.3
N-P1-L1000-T250	Class1	263.8	N-P2-L1000-T250	Class2	197.6	N-P3-L1000-T250	Class4	105.7
N-P1-L1000-T300	Class1	236.1	N-P2-L1000-T300	Class2	176.9	N-P3-L1000-T300	Class3	96.7
N-P1-L1000-T350	Class1	199.2	N-P2-L1000-T350	Class1	149.3	N-P3-L1000-T350	Class3	84.9
N-P1-L1000-T400	Class1	122.1	N-P2-L1000-T400	Class1	91.5	N-P3-L1000-T400	Class2	55.6
N-P1-L1000-T450	Class1	86.2	N-P2-L1000-T450	Class1	64.6	N-P3-L1000-T450	Class1	42.3
N-P1-L1000-T500	Class1	34.5	N-P2-L1000-T500	Class1	25.9	N-P3-L1000-T500	Class1	17.2
N-P1-L1000-T600	Class1	13.6	N-P2-L1000-T600	Class1	10.3	N-P3-L1000-T600	Class1	6.8
N-P1-L2000-T24	Class1	235.3	N-P2-L2000-T24	Class3	176.0	N-P3-L2000-T24	Class4	115.9
N-P1-L2000-T100	Class1	231.3	N-P2-L2000-T100	Class3	173.0	N-P3-L2000-T100	Class4	113.7
N-P1-L2000-T200	Class1	204.0	N-P2-L2000-T200	Class2	152.6	N-P3-L2000-T200	Class4	100.3
N-P1-L2000-T250	Class1	187.7	N-P2-L2000-T250	Class2	144.8	N-P3-L2000-T250	Class4	92.6
N-P1-L2000-T300	Class1	169.8	N-P2-L2000-T300	Class2	127.0	N-P3-L2000-T300	Class3	84.0
N-P1-L2000-T350	Class1	146.8	N-P2-L2000-T350	Class1	109.8	N-P3-L2000-T350	Class3	72.8
N-P1-L2000-T400	Class1	97.9	N-P2-L2000-T400	Class1	73.3	N-P3-L2000-T400	Class2	48.7
N-P1-L2000-T450	Class1	72.0	N-P2-L2000-T450	Class1	54.0	N-P3-L2000-T450	Class1	35.9
N-P1-L2000-T500	Class1	31.2	N-P2-L2000-T500	Class1	23.3	N-P3-L2000-T500	Class1	15.6
N-P1-L2000-T600	Class1	13.3	N-P2-L2000-T600	Class1	10.0	N-P3-L2000-T600	Class1	6.6

471

472 Table.8. Numerical ultimate strengths of FE model at elevated temperatures of Series N-L

Specimen (H/t=15, B/t=8)	Classification of cross-sections	P_{FE}(kN)	Specimen (H/t=20, B/t=10)	Classification of cross-sections	P_{FE}(kN)	Specimen (H/t=30, B/t=15)	Classification of cross-sections	P_{FE}(kN)
N-L1-L360-T24	Class1	409.0	N-L2-L360-T24	Class3	294.4	N-L3-L360-T24	Class4	178.5
N-L1-L360-T100	Class1	401.0	N-L2-L360-T100	Class3	289.3	N-L3-L360-T100	Class4	175.8
N-L1-L360-T200	Class1	353.5	N-L2-L360-T200	Class2	255.1	N-L3-L360-T200	Class4	155.1
N-L1-L360-T250	Class1	317.7	N-L2-L360-T250	Class2	231.2	N-L3-L360-T250	Class4	142.1
N-L1-L360-T300	Class1	283.2	N-L2-L360-T300	Class2	207.1	N-L3-L360-T300	Class3	127.9
N-L1-L360-T350	Class1	239.5	N-L2-L360-T350	Class1	176.0	N-L3-L360-T350	Class3	110.1
N-L1-L360-T400	Class1	148.0	N-L2-L360-T400	Class1	108.1	N-L3-L360-T400	Class2	67.5
N-L1-L360-T450	Class1	105.0	N-L2-L360-T450	Class1	77.0	N-L3-L360-T450	Class1	48.7
N-L1-L360-T500	Class1	40.2	N-L2-L360-T500	Class1	30.0	N-L3-L360-T500	Class1	19.7
N-L1-L360-T600	Class1	15.9	N-L2-L360-T600	Class1	11.9	N-L3-L360-T600	Class1	7.9
N-L1-L1000-T24	Class1	381.6	N-L2-L1000-T24	Class3	280.5	N-L3-L1000-T24	Class4	176.0
N-L1-L1000-T100	Class1	376.5	N-L2-L1000-T100	Class3	277.2	N-L3-L1000-T100	Class4	173.4
N-L1-L1000-T200	Class1	332.1	N-L2-L1000-T200	Class2	244.5	N-L3-L1000-T200	Class4	153.0
N-L1-L1000-T250	Class1	301.8	N-L2-L1000-T250	Class2	222.5	N-L3-L1000-T250	Class4	140.3
N-L1-L1000-T300	Class1	270.6	N-L2-L1000-T300	Class2	199.4	N-L3-L1000-T300	Class3	126.4
N-L1-L1000-T350	Class1	230.1	N-L2-L1000-T350	Class1	170.7	N-L3-L1000-T350	Class3	109.0
N-L1-L1000-T400	Class1	140.6	N-L2-L1000-T400	Class1	103.8	N-L3-L1000-T400	Class2	67.1
N-L1-L1000-T450	Class1	100.3	N-L2-L1000-T450	Class1	73.9	N-L3-L1000-T450	Class1	48.0
N-L1-L1000-T500	Class1	39.6	N-L2-L1000-T500	Class1	29.6	N-L3-L1000-T500	Class1	19.5
N-L1-L1000-T600	Class1	15.6	N-L2-L1000-T600	Class1	11.7	N-L3-L1000-T600	Class1	7.7
N-L1-L2000-T24	Class1	300.3	N-L2-L2000-T24	Class3	224.2	N-L3-L2000-T24	Class4	146.6
N-L1-L2000-T100	Class1	295.3	N-L2-L2000-T100	Class3	220.5	N-L3-L2000-T100	Class4	144.0
N-L1-L2000-T200	Class1	260.7	N-L2-L2000-T200	Class2	194.6	N-L3-L2000-T200	Class4	127.2
N-L1-L2000-T250	Class1	240.3	N-L2-L2000-T250	Class2	179.4	N-L3-L2000-T250	Class4	117.3
N-L1-L2000-T300	Class1	217.0	N-L2-L2000-T300	Class2	162.0	N-L3-L2000-T300	Class3	106.1
N-L1-L2000-T350	Class1	189.2	N-L2-L2000-T350	Class1	141.4	N-L3-L2000-T350	Class3	92.7
N-L1-L2000-T400	Class1	119.3	N-L2-L2000-T400	Class1	89.3	N-L3-L2000-T400	Class2	58.9
N-L1-L2000-T450	Class1	85.7	N-L2-L2000-T450	Class1	64.1	N-L3-L2000-T450	Class1	42.6
N-L1-L2000-T500	Class1	36.2	N-L2-L2000-T500	Class1	27.1	N-L3-L2000-T500	Class1	18.0
N-L1-L2000-T600	Class1	15.0	N-L2-L2000-T600	Class1	11.3	N-L3-L2000-T600	Class1	7.5

473

474 Table. 9. Comparisons between numerical results and design predictions for Series H-P

Specimens (Number of specimens: 90)	Comparisons				
	$\frac{P_{FE}}{P_{AA-1}}$	$\frac{P_{FE}}{P_{AA-2}}$	$\frac{P_{FE}}{P_{AS/NAS-1}}$	$\frac{P_{FE}}{P_{EC9-1}}$	$\frac{P_{FE}}{P_{EC9-2}}$
Mean, P_m	1.00	6.26	1.04	1.12	5.48
CoV, V_P	0.070	1.067	0.104	0.060	0.907
Resistance factor, ϕ	0.85	0.85	0.85	0.91	0.91
Reliability index, β	2.87	2.27	2.67	2.96	2.39

475

476

477 Table. 10. Comparisons between numerical results and design predictions for Series H-L

Specimens (Number of specimens: 90)	Comparisons				
	$\frac{P_{FE}}{P_{AA-1}}$	$\frac{P_{FE}}{P_{AA-2}}$	$\frac{P_{FE}}{P_{AS/NAS-1}}$	$\frac{P_{FE}}{P_{EC9-1}}$	$\frac{P_{FE}}{P_{EC9-2}}$
Mean, P_m	1.07	6.86	1.12	1.26	6.05
CoV, V_P	0.048	1.049	0.082	0.089	0.885
Resistance factor, ϕ	0.85	0.85	0.85	0.91	0.91
Reliability index, β	3.24	2.39	3.09	3.30	2.56

478

479

480

481 Table. 11. Comparisons between numerical results and design predictions for Series N-P

Specimens (Number of specimens: 90)	Comparisons				
	$\frac{P_{FE}}{P_{AA-1}}$	$\frac{P_{FE}}{P_{AA-2}}$	$\frac{P_{FE}}{P_{AS/NAS-1}}$	$\frac{P_{FE}}{P_{EC9-1}}$	$\frac{P_{FE}}{P_{EC9-2}}$
Mean, P_m	1.01	3.22	1.06	1.05	2.29
CoV, V_P	0.066	0.631	0.102	0.047	0.472
Resistance factor, ϕ	0.85	0.85	0.85	0.91	0.91
Reliability index, β	2.94	2.72	2.76	2.70	2.64

482

483

484

485 Table. 12. Comparisons between numerical results and design predictions for Series N-L

Specimens (Number of specimens: 90)	Comparisons				
	$\frac{P_{FE}}{P_{AA-1}}$	$\frac{P_{FE}}{P_{AA-2}}$	$\frac{P_{FE}}{P_{AS/NAS-1}}$	$\frac{P_{FE}}{P_{EC9-1}}$	$\frac{P_{FE}}{P_{EC9-2}}$
Mean, P_m	1.08	3.48	1.13	1.23	2.61
CoV, V_P	0.049	0.621	0.083	0.086	0.448
Resistance factor, ϕ	0.85	0.85	0.85	0.91	0.91
Reliability index, β	3.27	2.87	3.15	3.22	3.01

486

487